**Article ID:** 1000-324X(2023)10-1237-08 **DOI:** 10.15541/jim20230095

# Adsorption Mechanism of NaY Zeolite Molecular Adsorber Coating on Typical Space Contaminations

DAI Jieyan[1,2], FENG Aihu[2], MI Le[2], YU Yang[2], CUI Yuanyuan[3], YU Yun[1,2]

(1. College of Chemistry and Materials Science, Shanghai Normal University, Shanghai 200234, China; 2. Shanghai Institute of Ceramics, Chinese Academy of Sciences, Shanghai 201899, China; 3. School of Materials Science and Engineering, Shanghai University, Shanghai, 200444, China)

**Abstract:** In a high vacuum environment, some organic molecular pollutants such as hydrocarbon and siloxane are released by spacecraft materials and deposited on the surface of the sensitive parts of spacecraft devices, which has become an important adverse factor restricting the development of long-life and high-performance spacecraft. Zeolite molecular adsorber coating can effectively collect spatial contaminations in real time, but the adsorption mechanism is not clear. To deeply analyze the adsorption mechanism of zeolite on the spatial contaminations, the adsorption behaviors of NaY zeolite including adsorption isotherms, adsorption heat curves and density distributions on three typical contaminations, toluene($C_7H_8$), dimethyl phthalate ($C_{10}H_{10}O_4$), octamethyl cyclotetrasiloxane ($C_8H_{24}O_4Si_4$), were calculated by the Grand Canonical Monte Carlo method in this work. The NaY zeolites and pollutant models were successfully constructed, and the rationality of the models was verified by comparing simulated data with experimental ones. These results indicated that all three classic molecules can be adsorbed by NaY zeolite in the ultra-high vacuum condition. The saturated adsorption capacity decreases in the order of $C_7H_8$>$C_{10}H_{10}O_4$>$C_8H_{24}O_4Si_4$, which is significantly related to the molecule sizes and structures of contaminations. The saturated adsorption amount of $C_8H_{24}O_4Si_4$ is relatively low (8 per cell) when that of $C_7H_8$ is 36 per cell. In addition, the density distributions indicates that different contaminations are preferentially adsorbed inside the super-cage of NaY zeolite. Overall, this work analyzes the adsorption mechanism of NaY zeolite on typical contaminations, and can provide basic insights for the development of zeolite molecular adsorber coating with high adsorption capacity.

**Key words:** Monte Carlo simulation; NaY zeolites; adsorption mechanism; space contaminants

In a high vacuum space environment, the molecular contaminants released by some organic space materials[1-3], such as plastics, adhesives, lubricants, silicones, epoxies, potting compounds, and other similar materials, deposit on the surface of sensitive optical components, thermal control components, and solar panels, which seriously affects the performance and service life of the spacecraft[4-6]. At the same time, the molecular contaminants mentioned above also pollute the manned cabins to affect the equipment in the cabin and the health of astronauts[7-8]. Conventional methods such as selecting low outgassing materials and increasing the number of thermal vacuum bake on the ground can no longer meet the design requirements of long-life spacecraft. The problem of on-orbit molecular pollution has become an important unfavorable factor to restrict the development of long-life and high-performance spacecraft. It is urgent to develop new technologies to control space contaminations[9-12].

Thanks to the rich pore structure, porous adsorbents can collect space contaminations in real time[13]. As a space adsorbent material, in addition to the molecular adsorption function, it is also required to have good space environmental stability and low outgassing performance. Zeolite molecular sieve is an inorganic

**Received date:** 2023-02-25; **Revised date:** 2023-03-25; **Published online:** 2023-06-01
**Foundation item:** National Natural Science Foundation of China (52202076); Youth Innovation Promotion Association CAS (2023261); Shanghai "Super Postdoctoral Fellow" Incentive Program (2020474)
**Biography:** DAI Jieyan (1997–), female, Master candidate. E-mail: daijieyan25@163.com
戴洁燕(1997–), 女, 硕士研究生. E-mail: daijieyan25@163.com
**Corresponding author:** FENG Aihu, associate professor. E-mail: fengaihu@mail.sic.ac.cn; YU Yun, professor. E-mail: yunyush@mail.sic.ac.cn
冯爱虎, 副研究员. E-mail: fengaihu@mail.sic.ac.cn; 于 云, 研究员. E-mail: yunyush@mail.sic.ac.cn

adsorbent material with good space environmental stability which can withstand harsh environments such as space particle irradiation and atomic oxygen erosion. The zeolite molecular adsorber coating (MAC) is one kind of new and innovative materials, which is developed by National Aeronautics and Space Administration (NASA) to reduce the risk of space contaminations[2, 14]. The advantage of zeolite molecular adsorber coating is that it can effectively collect molecular contaminants in real time, and when the contaminant molecules move to the surface and inside the coating, they will be effectively adsorbed by the zeolite adsorbent. As a porous inorganic material coating, MAC mainly includes inorganic zeolite filler and inorganic silica sol binder. It offers impressive absorptive capabilities for different contaminants[15]. In the extreme ultra-high vacuum and variable temperature space environment, the capturing and adsorbing process of zeolite on contaminants are more complicated. However, the current research on zeolite MAC is still mainly based on the experimental test of the adsorption capacity, and the in-depth analysis of the adsorption and diffusion processes of contaminant molecules in zeolites is still lacking in the on-orbit environment. Therefore, the MAC with ultra-high adsorption capacity cannot be individually designed for different space missions. Computational simulation is a good substitute for experimental testing to efficiently explore the adsorption process of zeolite on different contaminants in ultra-high vacuum conditions[16-19].

The main volatiles of aerospace cables, silicone rubber, rubber gaskets, *etc*. are toluene, phthalates, and siloxane molecules, and the models of some typical organic molecules, including toluene, dimethyl phthalate and octamethyl cyclotetrasiloxane were established by the Material Studio in this work, and the X-ray diffraction patterns and adsorption process of NaY zeolite were calculated and compared with the experiment data. In order to study the adsorption process of the contaminants under the on-orbit environment, the adsorption isotherm, adsorption heat and density distribution of different contaminants in NaY zeolite also were calculated and predicted. This work could provide some theoretical data for the development and individual design of zeolite molecular adsorber coating.

# 1 Simulation details

## 1.1 Contaminant models

In this work, toluene($C_7H_8$), dimethyl phthalate ($C_{10}H_{10}O_4$), octamethyl cyclotetrasiloxane ($C_8H_{24}O_4Si_4$) were used as target contaminants. As shown in Fig. 1, these contaminant models were established by using Material Studio software package.

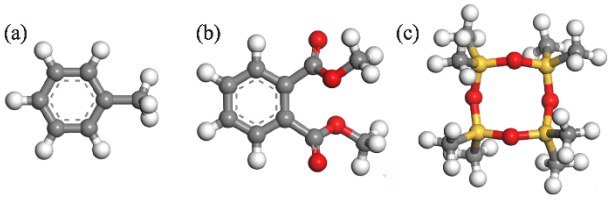


Fig. 1 Three different contaminant models
(a) $C_7H_8$; (b) $C_{10}H_{10}O_4$; (c) $C_8H_{24}O_4Si_4$

## 1.2 NaY zeolite models

An original FAU zeolite with the chemical composition of $Si_{96}Al_{96}O_{384}$ was established by the Material Studio software package, and its Si/Al ratio was 1:1. The space group of original FAU zeolite was Fd-3z, $a=b=c$=25.028 Å, $\alpha=\beta=\gamma$=90°[20-21]。Then 42 aluminum atoms were changed randomly to Si atoms in accordance with the Si/Al ratio (2.6) of the experiment NaY zeolite and the substituting process must satisfy the Löwenstein rule. 54 sodium atoms need to be introduced for charge balance by three different ways. The first method refers to the distribution rule of cations reported in the literatures[22-23]. The monovalent alkali metal ions of NaY zeolite occupied the sites of Ⅰ, Ⅰ′ and Ⅱ, and SⅡ (site of Ⅱ) was close to being fully occupied, when SⅠ (site of Ⅰ) and SⅠ′ (site of Ⅰ′) were occupied partly. Therefore, for 54 sodium ions in this work, 32 of them firstly occupied the SⅡ. As for the distribution of SⅠ and SⅠ′, some different attempts were tried. Then the geometric structures of different NaY zeolites were optimized by using the Forcite module in the Material Studio software. With respect to the second way, sodium atoms were randomly placed one by one and the zeolites with the lowest energy were optimized in 54 times. In the third way, sodium atoms were placed randomly and then the zeolite was optimized in one time. NaY zeolites with the composition of $Na_{54}Si_{138}Al_{54}O_{384}$ and the Si/Al ratio of 2.6 were established and different optimized zeolites above were named NaY2.6 opt1, NaY2.6 opt2, NaY2.6 opt3, respectively. The final sites of 54 sodium ions of NaY opt1 were 32SⅡ, 13SⅠ, 8SⅠ′ and 1SⅢ′, and the distributions of sodium ions in NaY opt2 and NaY opt3 zeolite structures were 2SⅠ, 19SⅠ′, 30SⅡ, 2SⅢ, 1SⅢ' and 5SⅠ, 12SⅠ′, 15SⅡ, 9SⅢ, 13SⅢ′, respectively. The NaY zeolite was semi-ionic with atoms carrying the following partial charges: Si(+2.4e), Al(+1.4e), O(–1.2e), Na(+1e)[24-25]. The structures of three NaY zeolites were shown in Fig. 2.

## 1.3 Adsorption process

Grand Canonical Monte Carlo (GCMC) technique was applied to simulate the adsorption process between NaY

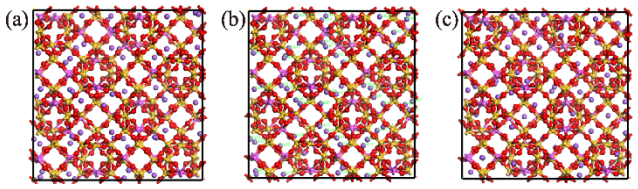


Fig. 2　Three NaY models
(a) NaY2.6 opt1; (b) NaY2.6 opt2; (c) NaY2.6 opt3
The balls have four colors including purple, yellow, pink, and red, representing atoms of sodium, silicon, aluminum, and oxygen, respectively

zeolite and different adsorbates[19, 26]. This technique is in the constant μVT ensemble, which means chemical potential, volume and temperature of the whole system are fixed. The force fields used as calculating potential energy of the system are the force between atoms or molecules of the studied system, including bonded and non-bonded interactions. The interactions between zeolites and other three absorbates as well as between adsorbates and adsorbates took place through the non-bonded energy which is the sum of van der Waals interaction and the electrostatic energy by the Formula (1) when the former is expressed by Lennard-Jones (LJ) potential energy and the latter is expressed by Ewald method calculation[26-27]:

$$U(r_{ij}) = 4\varepsilon_{ij} \times \left[ \left( \frac{\sigma_{ij}}{r_{ij}} \right)^{12} - \left( \frac{\sigma_{ij}}{r_{ij}} \right)^{6} \right] + \frac{q_i q_j}{4\pi\varepsilon_0 r_{ij}} \qquad (1)$$

where $U$ is total potential energy, $r_{ij}$ is the distance between atoms i and j, $\varepsilon_{ij}$ and $\sigma_{ij}$ are the LJ potential parameters, $\varepsilon_0$ is the vacuum permittivity ($\varepsilon_0$=8.85×10$^{-12}$ C$^2$·N$^{-1}$·m$^{-2}$), $q_i$ and $q_j$ are the partial charges for atoms i and j. The box length of NaY zeolite along each direction was longer than 24 Å. So a cut off distance of 12 Å was applied to all LJ interactions[28-29]. The long-range electrostatic interactions were accounted for using the Ewald sum technique.

The number of molecules or atoms in the simulation process directly determines the running speed and ability of the computer, and the amount of calculation could be reduced by setting valid boundary conditions in all three directions. Therefore, only one zeolite crystal cell with 1×1×1 was used as a simulated unit. Meanwhile, the skeleton atoms including silicon atoms and aluminum atoms were fixed at the coordinate position. The contaminant molecules remained rigid, and these molecules could only move and rotate without deformation in the simulation process.

In this work, the Sorption module and COMPASS force-field in Material Studio simulation package were used to calculate the adsorption process of NaY zeolites on different contaminants[30-31]. The Monte Carlo interactions were set to 1×10$^7$ when the first 5×10$^6$ steps were calculated only for equilibration and the second 5×10$^6$ steps were calculated for predicting the adsorption capacity.

## 2　Materials and Experimental details

NaY zeolite was purchased from Nankai University Catalyst Co., Ltd. (China). The phase of NaY zeolite samples was studied by Bruker D2 PHASER powder diffractometer with Cu K$\alpha$ radiation operated at 40 kV and 200 mA. Toluene adsorption isotherm of NaY zeolite was measured by the Intelligent Gravimetric Analyzer (3H2000-PW, Beishide Instrument Technology (Beijing) Co., Ltd) at 298 K, and the sample in the vessel was vacuumed up to 105 mbar and outgassed at 573 K for 24 h before measurements.

## 3　Results and discussion

### 3.1　Toluene adsorption

The established NaY zeolite models are verified by comparing the simulated X-ray diffraction patterns with the actual measurement. As shown in Fig. 3, the characteristic peaks of three NaY zeolite models calculated by the Reflex Module of Material Studio are very similar[26], which are 10°, 11.75°, 15.45°, 18.4°, 20.05°, 23.3°, 26.65°, 30.3°, and 30.95°. The experimental characteristic peaks of NaY zeolite are 10.13°, 11.88°, 15.63°, 18.65°, 20.33°, 23.61°, 27.01°, 30.7°, and 31.34°. Therefore, the diffraction peak positions of simulated XRD patterns are highly consistent with the experimental results, indicating that the NaY zeolite models meet the simulation requirements.

The experimental result of toluene adsorption isotherms and the simulated adsorption isotherms of three NaY zeolites at 298 K are demonstrated in Fig. 4. It can also be seen that the three simulated NaY zeolites have a similar trend, rising rapidly at low pressure and

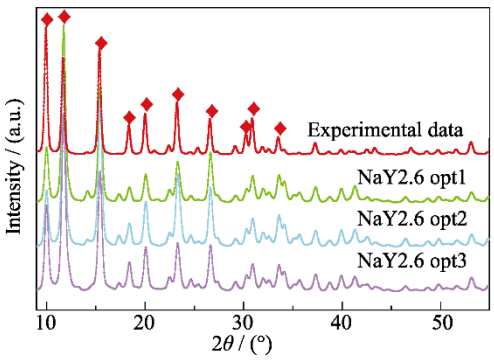


Fig. 3　Comparison between simulated and experimental results of X-ray diffraction patterns

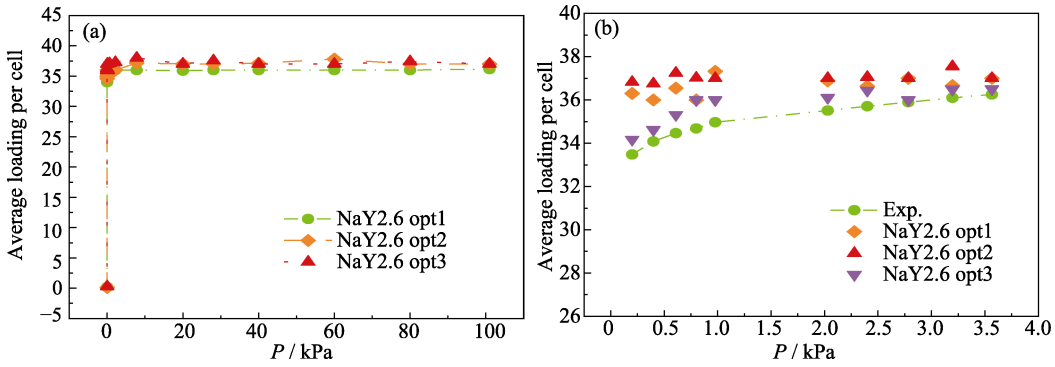


Fig. 4 Adsorption isotherms of NaY zeolite on toluene at 298 K
(a) Simulated data; (b) Experimental data

remaining stable with the pressure increasing. The saturated toluene adsorption capacity simulated by different NaY zeolite models is about 36 per cell, which is close to the experimental data (36.2 per cell) in Fig. 4(b) and other simulated data in the literatures[20, 36-37] in Table 1. It is important to note that the saturated adsorption isotherm of NaY opt3 is sufficiently accurate in respect of the experimental data.

Considering the convenience of establishing NaY zeolites models and the validation of simulation method, the NaY2.6 opt3 model is the most suitable one, which is selected as the targeted simulation model in the following calculation of adsorption process.

Temperature and pressure are two significant factors in the space environment, and different temperatures (173, 223, 273, 298, and 373 K) in the range from ultra-high vacuum to standard atmospheric pressure are applied to simulate the adsorption capacity of NaY zeolite on toluene. As shown in Fig. 5, due to the limitation of the total pore volume, the adsorption capacity of toluene cannot be increased by adjusting the temperature and pressure at relatively high pressures (1 Pa<$P$<101 kPa). Temperature has little influence on the toluene adsorption capacity of NaY zeolite that is kept at about 36 per cell. However, in the range of low pressure ($P$<1 Pa), as the temperature increasing, the adsorption capacity of NaY zeolite shows a great difference in Fig. 5(b), and the toluene adsorption capacity at high temperature is smaller than that at low temperature. When pressure is lower than $10^{-7}$ kPa, the adsorption capacity at 373 K is close to zero while that is about 25 per cell at 298 K. The adsorption capacity is basically maintained at 36 per cell at lower temperatures.

The adsorption heat of NaY zeolite on toluene were simulated and shown in Fig. 5(c). It can be observed that the adsorption heat is about 105 kJ/mol, which is close to the experimental data (95 kJ/mol) measured by temperature-programmed desorption method[34] and the simulated data (105.5 kJ/mol)[35], representing the strong interactions between toluene and NaY zeolite. In addition, the adsorption heat decreases from 111 kJ/mol (173 K, $10^{-7}$ kPa) to 94 kJ/mol (373 K, $10^{-7}$ kPa) at low pressure. With the increase of pressure, the adsorption heat and the adsorption capacity are kept at about 110 kJ/mol and 36 per cell, respectively. Temperature influences the interaction between toluene and NaY zeolite, which can be expressed by the wave form of the adsorption heat. At low pressure, the adsorption capacity is relatively stronger, while the desorption is more difficult, resulting in a higher adsorption capacity. Overall, the NaY zeolite has a bright application prospect in high vacuum condition.

In order to further understand the adsorption behaviors of NaY zeolites on toluene, the density distributions were investigated. As shown in Fig. 6, different density distributions are represented at the pressure of $10^{-6}$ Pa,

**Table 1 Comparison of adsorption capacity of different FAU zeolite on toluene**

| Number | Type | Zeolite | Adsorbate | Pressure/kPa | Temperature/K | Adsorption amount | Ref. |
|---|---|---|---|---|---|---|---|
| 1 | Simulation | FAU | Toluene | 0.0022 | 298 | 28 per cell | [36] |
| 2 | Simulation | FAU | Toluene | 100 | 298 | 30 per cell | [20] |
| | Simulation | FAU | Toluene | 100 | 350 | 30 per cell | |
| 3 | Simulation | FAU-NaY | Toluene | 1.5 | 300 | ~2.5 mmol/g (248 mg/g) | [37] |
| 4 | Simulation | FAU-NaY | Toluene | 101 | 298 | ~36 per cell (260 mg/g) | This work |
| | Simulation | FAU-NaY | Toluene | 101 | 373 | ~36 per cell | |
| | Experiment | FAU-NaY | Toluene | 3.6 | 298 | 36.3 per cell (262 mg/g) | |

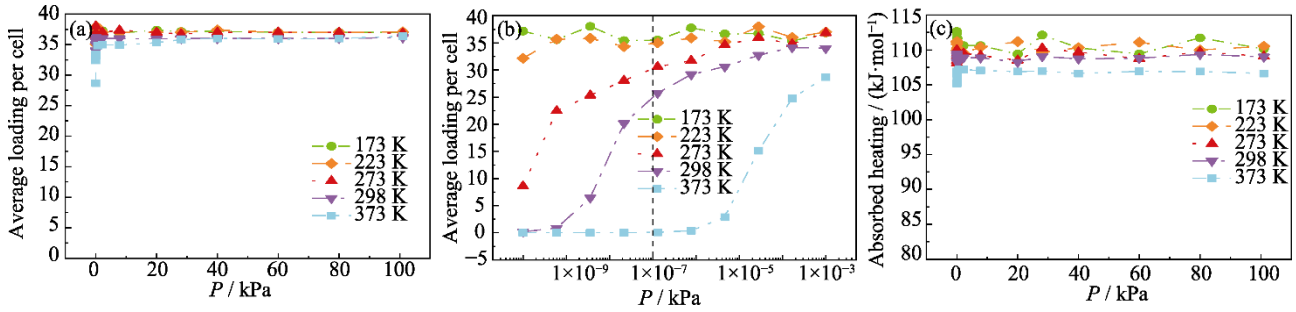


Fig. 5　Simulated toluene adsorption isotherms of NaY zeolite at different pressures
(a) $10^{-3}$–101 kPa; (b) $10^{-10}$–$10^{-3}$ kPa; (c) Adsorption heat of NaY zeolites

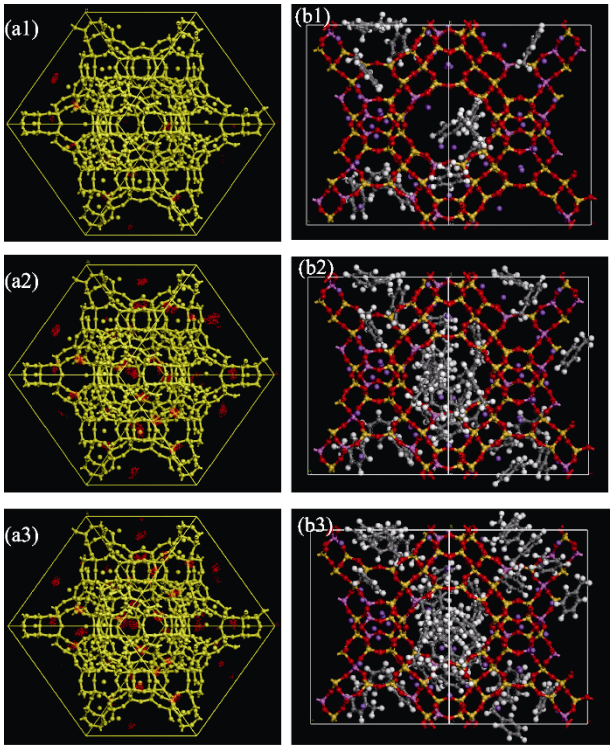


Fig. 6　Density distribution of toluene in NaY zeolite at different pressures
(a1, b1) $10^{-6}$ Pa; (a2, b2) $10^{-4}$ Pa; (c1, c2) 1 Pa

$10^{-4}$ Pa, and 1 Pa, respectively. The yellow ball and stick model are the NaY zeolite framework and the red scatter plots represent the presence possibility of toluene in Fig. 6. It can be seen that adsorption locates of toluene in NaY zeolites are distributed along with the interior of super-cage, especially close to twelve-membered ring. There are no toluene molecules existing in the sodalite cage (Fig. 7) due to the toluene size (6.3 Å) is close to the diameter of six-membered ring of sodalite cage and smaller than that of super-cage (12 Å). With the increase of pressure, more and more toluene molecules are adsorbed inside the super-cage, including the position near twelve-membered ring and the center of super-cage in Fig. 6.

## 3.2　$C_{10}H_{10}O_4$ and $C_8H_{24}O_4Si_4$ adsorption

As shown in Fig. 8, the adsorption capacity of NaY

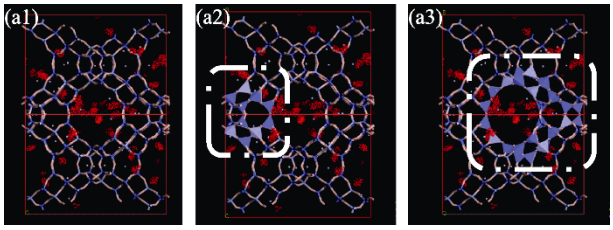


Fig. 7　Density distribution of toluene in NaY zeolite at pressure of 1 Pa
(a1) Density distribution image with different visual angle compared with Fig. 6(a3); (a2) Density distribution in $\beta$ cage; (a3) Density distribution in super-cage

zeolite on $C_{10}H_{10}O_4$ and $C_8H_{24}O_4Si_4$ molecules were calculated at different temperatures and pressures. With the increase of temperature, the adsorption capacity of NaY zeolite for $C_{10}H_{10}O_4$ and $C_8H_{24}O_4Si_4$ demonstrate obvious differences in the range of different pressures. In the range of low pressure ($P$<1 Pa), the adsorption capacity of two molecules is really influenced by temperature. The adsorption capacity of NaY zeolite on $C_{10}H_{10}O_4$ is only about 17 per cell when temperature up to 473 K. Similarly, the $C_8H_{24}O_4Si_4$ adsorption capacity reduces when temperature up to 348 K. However, the adsorption capacity of NaY zeolite on two contaminants still maintains a high value when the pressure is $10^{-7}$ kPa. In the higher pressure range (1 Pa<$P$<101 kPa), the adsorption capacity of two molecules is basically unchanged with the increase of temperature, and the saturated adsorption capacity is about 17 per cell ($C_{10}H_{10}O_4$) and 8 per cell ($C_8H_{24}O_4Si_4$), respectively.

The adsorption heat of NaY zeolite on $C_{10}H_{10}O_4$ and $C_8H_{24}O_4Si_4$ was studied at different temperatures in Fig. 9. The adsorption heat of $C_8H_{24}O_4Si_4$ decreases with the increase of temperature, while that of $C_{10}H_{10}O_4$ changes slightly with different temperatures. The difference of adsorption heat is related to the structure of $C_{10}H_{10}O_4$ and $C_8H_{24}O_4Si_4$. Compared with toluene, the molecular structures of $C_{10}H_{10}O_4$ and $C_8H_{24}O_4Si_4$ are more complex and larger, resulting in higher adsorption heat and smaller adsorption capacity.

In Fig. 10, density distributions of $C_{10}H_{10}O_4$ and

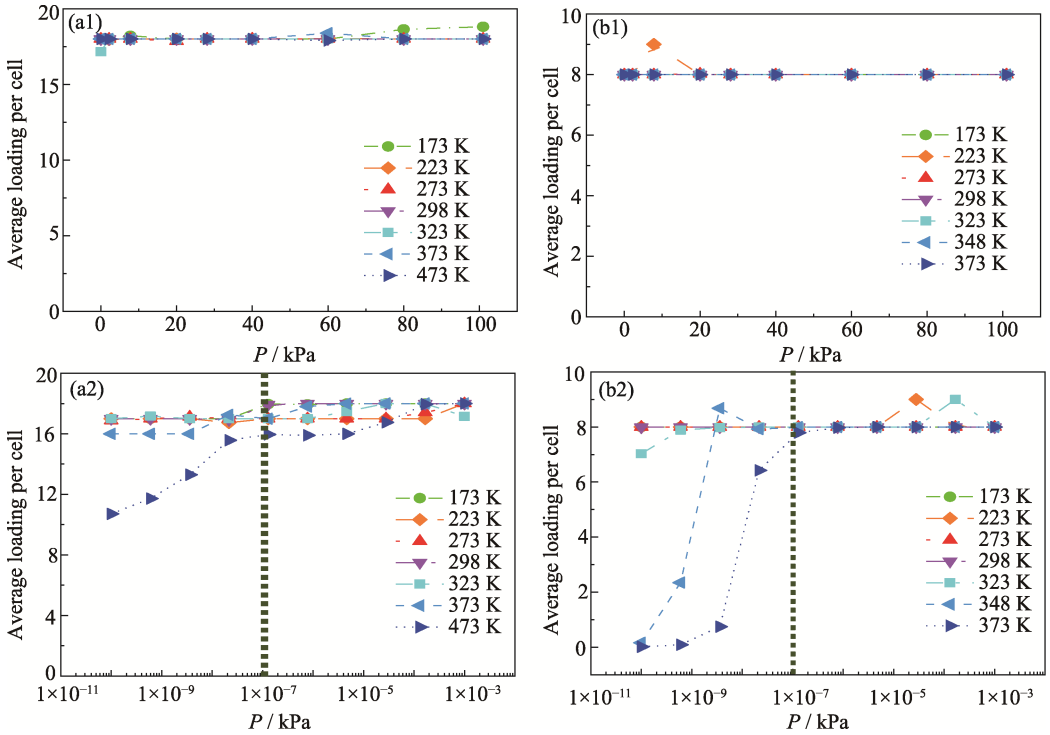


Fig. 8 Simulated adsorption isotherms of NaY zeolites at different pressures
(a) $C_{10}H_{10}O_4$; (b) $C_8H_{24}O_4Si_4$

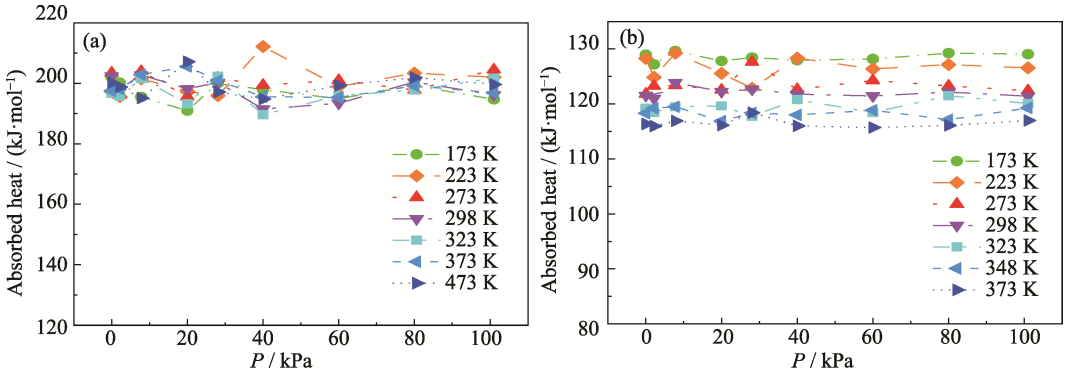


Fig. 9 Adsorption heat of NaY zeolites at different temperatures
(a) $C_{10}H_{10}O_4$; (b) $C_8H_{24}O_4Si_4$

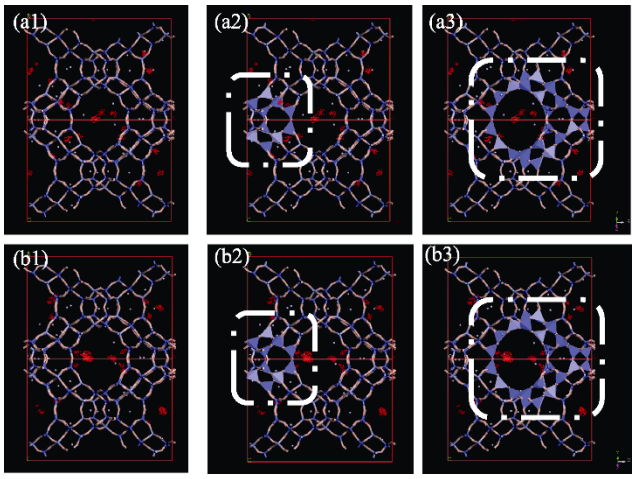


Fig. 10 Density distributions of $C_{10}H_{10}O_4$ (a) and $C_8H_{24}O_4Si_4$ (b) in NaY zeolite at pressure of 1 Pa (298 K)
(a1, b1) Original density distributions; (a2, b2) Density distributions in *β* cage; (a3, b3) Density distribution in the super-cage

$C_8H_{24}O_4Si_4$ at pressure of 1 Pa were demonstrated. It can be seen apparently that the adsorption sites of both molecules are distributed within super-cage rather than sodalite cage. Compared with the adsorption behavior on toluene (Fig. 7), the red scatter plots in Fig. 10 are less and distributions of two molecules are more concentrated. Considering the larger cell diameter and more complex structures of $C_{10}H_{10}O_4$ and $C_8H_{24}O_4Si_4$, this result is reasonable.

## 4 Conclusions

In this work, the models of NaY zeolite and different contaminants were established successfully. The effects of temperature and pressure on the adsorption capacity and adsorption heat on different molecules were carefully studied. Three molecules including toluene, dimethyl

phthalate and octamethyl cyclotetrasiloxane exhibit different adsorption capacities on NaY zeolite and the values were about 36 per cell, 17 per cell and 8 per cell, respectively, which is related to their molecular structures. These contaminants can be effectively adsorbed by NaY zeolite under ultra-high vacuum situation, so the molecular adsorber coating based on NaY zeolite has a significant application prospect.

## References:


[1] LIMERO T, REESE E, CHENG P, *et al*. Preparation of a gas chromatograph-differential mobility spectrometer to measure target volatile organic compounds on the international space station. *International Journal for Ion Mobility Spectrometry*, 2011, **14(2):** 81.

[2] ABRAHAM N S, HASEGAWA M M, SECUNDA M S. Application of the molecular adsorber coating technology on the Ionospheric Connection Explorer Program. *Proceedings of SPIE*, 2016, **9952:** 99520D.

[3] LIMERO T, REESE E, WALLACE W T, *et al*. Results from the air quality monitor (gas chromatograph-differential mobility spectrometer) experiment on board the international space station. *International Journal for Ion Mobility Spectrometry*, 2012, **15(3):** 189.

[4] SANDERS J T. Molecular contamination of an EUV instrument in geosynchronous orbit. *Proceedings of SPIE*, 2004, **5526:** 44.

[5] CANHAM J S. Revisiting mechanisms of molecular contamination induced laser optic damage. *Proceedings of SPIE*, 2007, **6720:** 67200M.

[6] CHANG C W, KANNENBERG K, CHIDESTER M H. Development of versatile molecular transport model for modeling spacecraft contamination. *Proceedings of SPIE*, 2010, **7794:** 77940O.

[7] GUO S S, AI W D, FEI J X, *et al*. Study on the kinetic characteristics of trace harmful gases for a two-person-30-day integrated CELSS test. *Environmental Science and Pollution Research*, 2015, **22(9):** 7020.

[8] SNITKA V, BATIUSKAITE D, BRUZAITE I, *et al*. Surface-enhanced Raman scattering sensors for biomedical and molecular detection applications in space. *CEAS Space Journal*, 2021, **13(3):** 509.

[9] SHIMOSAKO N, EGASHIRA T, YOSHINO K, *et al*. Effects of vacuum on photocatalytic activity of $TiO_2$. *Proceedings of SPIE*, 2018, **10748:** 1074810.

[10] SHIMOSAKO N, YOSHINO K, SHIMAZAKI K, *et al*. Tolerance to electron beams of $TiO_2$ film photocatalyst. *Thin Solid Films*, 2019, **686:** 137421.

[11] DIBOUNE M, NOUALI H, SOULARD M, *et al*. Green hybrid zeolite coatings for on-orbit molecular decontamination. *Microporous and Mesoporous Materials*, 2020, **307:** 110478.

[12] SHIMOSAKO N, SAKAMA H. Influence of vacuum environment on photocatalytic degradation of methyl red by $TiO_2$ thin film. *Acta Astronaut*, 2021, **178:** 693.

[13] FENG A H, YU Y, MI L, *et al*. Synthesis and VOCs adsorption performance of surfactant-templated USY zeolites with controllable mesopores. *Chemical Physics Letters*, 2022, **798:** 139578.

[14] ABRAHAM N S, JALLICE D E. Preliminary testing of NASA's molecular adsorber coating technology for future missions to Mars. *Proceedings of SPIE*, 2018, **10748:** 107480E.

[15] STRAKA S, PETERS W, HASEGAWA M, *et al*. Development of molecular adsorber coatings. Conference on Optical System *Proceedings of SPIE*, 2010, **7794:** 77940C.

[16] CHEN H Y, XI H X, CAI X Y, *et al*. Experimental and molecular simulation studies of a ZSM-5-MCM-41 micro-mesoporous molecular sieve. *Microporous and Mesoporous Materials*, 2009, **118(1/2/3):** 396.

[17] MORADI H, AZIZPOUR H, BAHMANYAR H, *et al*. Effect of Si/Al ratio in the faujasite structure on adsorption of methane and nitrogen: a molecular dynamics study. *Chemical Engineering & Technology*, 2021, **44(7):** 1221.

[18] QIAO J, YANG S S, LI J J, *et al*. Dynamic simulation of deposition processes of spacecraft molecular contamination. *Tehnicki Vjesnik-Technical Gazette*, 2021, **28(1):** 321.

[19] WANG M Y, SHENG Y. Molecular simulation to analyze the influence of ultrafine particles on activated carbon adsorbing low concentration toluene. *Building and Environment*, 2022, **213:** 108875.

[20] ZHAO F, SUN X S, LU R F, *et al*. Adsorption of methanol, methanal, toluene, ethylbenzene, and styrene in zeolites: a grand canonical Monte Carlo simulation study. *Canadian Journal of Chemistry*, 2017, **95(12):** 1241.

[21] MORADI H, AZIZPOUR H, BAHMANYAR H, *et al*. Molecular dynamic simulation of carbon dioxide, methane, and nitrogen adsorption on Faujasite zeolite. *Chinese Journal of Chemical Engineering*, 2022, **43:** 70.

[22] MAURIN G, BELMABKHOUT Y, PIRNGRUBER G, *et al*. $CO_2$ adsorption in LiY and NaY at high temperature: molecular simulations compared to experiments. *Adsorption-Journal of the International Adsorption Society*, 2007, **13(5/6):** 453.

[23] PORCHER F, PAILLAUD J L, GABEROVA L, *et al*. Monitoring by *in situ* neutron diffraction of simultaneous dehydration and $Ni^{2+}$ mobility in partially exchanged NaY zeolites. *New Journal of Chemistry*, 2016, **40(5):** 4228.

[24] AMMOULI T, PAILLAUD J L, NOUALI H, *et al*. Insights into water adsorption in potassium-exchanged X-type faujasite zeolite: molecular simulation and experiment. *The Journal of Physical Chemistry C*, 2021, **125(35):** 19405.

[25] XIONG P, HE P, QU Y X, *et al*. The adsorption properties of NaY zeolite for separation of ethylene glycol and 1, 2-butanediol: experiment and molecular modelling. *Green Energy & Environment*, 2021, **6(1):** 102.

[26] SONG L Q, DU X S, CHEN Y R, *et al*. Screening of zeolites for $H_2S$ adsorption in mixed gases: GCMC and DFT simulations. *Microporous and Mesoporous Materials*, 2021, **328:** 111495.

[27] VUJIC B, LYUBARTSEV A P. Transferable force-field for modelling of $CO_2$, $N_2$, $O_2$ and Ar in all silica and $Na^+$ exchanged zeolites. *Modelling and Simulation in Materials Science and Engineering*, 2016, **24(4):** 045002.

[28] CHEN H Y, WANG W L, DING J, *et al*. $CO_2$ adsorption capacity of FAU zeolites in presence of $H_2O$: a Monte Carlo simulation study. *Energy Procedia*, 2017, **105:** 4370.

[29] HOU S Y, TANG Y L, ZHU T L, *et al*. Adsorptive removal of gas phase naphthalene on ordered mesoporous carbon. *Journal of Hazardous Materials*, 2022, **436:** 129208.

[30] RAHMATI M, MODARRESS H. Selectivity of new siliceous zeolites for separation of methane and carbon dioxide by Monte Carlo simulation. *Microporous and Mesoporous Materials*, 2013, **176:** 168.

[31] KEYVANLOO Z, POUR A N, MOOSAVI F, *et al*. Molecular dynamic simulation studies of adsorption and diffusion behaviors of methanol and ethanol through ZSM-5 zeolite. *Journal of Molecular Graphics & Modelling*, 2022, **110:** 108048.

[32] FENG A, YU Y, MI L, *et al*. Synthesis and characterization of hierarchical Y zeolites using $NH_4HF_2$ as dealumination agent. *Microporous and Mesoporous Materials*, 2019, **280:** 211.

[33] FENG A, YU Y, MI L, *et al*. Structural, textural and toluene adsorption properties of $NH_4HF_2$ and alkali modified USY zeolite. *Microporous and Mesoporous Materials*, 2019, **290:** 109646.

[34] YOSHIMOTO R, HARA K, OKUMURA K, *et al*. Analysis of toluene adsorption on Na-form zeolite with a temperature-programmed desorption method. *The Journal of Physical Chemistry C*, 2007, **111(3):** 1474.
[35] HESSOU E P, BEDE L A, JABRAOUI H, *et al*. Adsorption of toluene and water over cationic-exchanged Y zeolites: a DFT exploration. *Molecules*, 2021, **26(18):** 5486.
[36] ZHENG H M, ZHAO L, JI J J, *et al*. Unraveling the adsorption mechanism of mono- and diaromatics in faujasite zeolite. *ACS Applied Materials & Interfaces*, 2015, **7(19):** 10190.
[37] BRUNCHI C C, SANCHEZ J M C, STANKIEWICZ A I, *et al*. Adsorption of volatile organic compounds. experimental and theoretical study. *Industrial & Engineering Chemistry Research*, 2012, **51(51):** 16697.

# NaY 沸石分子吸附涂层对典型空间污染物的吸附机制研究

戴洁燕[1,2], 冯爱虎[2], 米 乐[2], 于 洋[2], 崔苑苑[3], 于 云[1,2]

(1. 上海师范大学 化学与材料科学学院, 上海 200234; 2. 中国科学院 上海硅酸盐研究所, 上海 201899; 3. 上海大学 材料科学与工程学院, 上海 200444)

**摘 要:** 在轨高真空环境下, 航天器所用非金属材料会释放出碳氢类、硅氧烷等有机分子污染物, 沉积在航天器光学系统等敏感表面, 影响航天器性能和使用寿命。沸石分子吸附涂层可以实时吸附空间污染物, 但对其吸附作用机制还缺乏深入研究。为深入分析空间污染物分子在沸石内部的吸附机制, 本工作采用巨正则蒙特卡洛方法模拟计算了 NaY 沸石对三种典型空间污染物(甲苯($C_7H_8$)、邻苯二甲酸二甲酯($C_{10}H_{10}O_4$)和八甲基环四硅氧烷($C_8H_{24}O_4Si_4$))的吸附行为(吸附等温线、吸附热曲线和粒子密度分布图)。模拟和实验数据的对比分析验证了计算模型和方法的合理性。在超高真空条件下, NaY 沸石对空间污染物表现出较高的吸附量, 但其饱和吸附量随着分子尺寸的增加而降低($C_7H_8$>$C_{10}H_{10}O_4$>$C_8H_{24}O_4Si_4$), 其中八甲基环四硅氧烷分子的饱和吸附量仅为 8 个分子, 远低于甲苯的 36 个分子。污染物分子在沸石内部的密度分布图显示, 三种污染物均优先吸附于 NaY 沸石的“超笼”位点。本研究系统分析了 NaY 沸石对典型污染物的吸附机制, 为高吸附性能的沸石分子筛吸附涂层的研发提供了理论指导。

**关 键 词:** 蒙特卡洛模拟; NaY 沸石; 吸附机理; 空间污染物

**中图分类号:** TQ174 **文献标志码:** A